Long-term variations and residual trends in the E, F and sporadic E (Es) layer over Juliusruh, Europe

M. Sivakandan[1], J. Mielich[1], T. Renkwitz[1], J. L. Chau[1], J. Jaen[1], and J. Lastovicka[2]

[1]Leibniz Institute of Atmospheric Physics at the University of Rostock (IAP), Kühlungsborn, Germany
[2]Institute of Atmospheric Physics Czech Academy of Sciences, Bocni II, 141 31, Praha, Czechia

Key Points:

- The amplitude of annual and solar cycle oscillations are predominant in the E-and F-region, respectively.
- In the E-region, daytime foE and foEs shows a weak negative trend during the period of 1964 to 2019.
- In the F-region, foF2 and hmF2 nighttime trend is larger than the daytime. Daytime foF2 trend is statistically insignificant.

Corresponding author: Sivakandan Mani, mani@iap-kborn.de

Abstract

In the present study, using sixty-three and fifty-six years of continuous observations, we investigate the long-term oscillations and residual trends, respectively, in the E- and F-region ionosonde measured parameters over Juliusruh, Europe. Using the Lomb-Scargle periodogram (LSP) long-term variations are estimated before the trend estimation. We found that the amplitude of the annual oscillation is higher than the 11-year solar cycle variation in the critical frequencies of the daytime E (foE) and Es (foEs) layers. A weak semi-annual oscillation is also identified in the foE. In the F-region, except for daytime hmF2, and nighttime foF2, the amplitude of the 11-year solar cycle variation is higher than the annual oscillation. The LSP estimated periods and their corresponding amplitudes are used to construct a model E- and F-region ionospheric parameters that are in good agreement with the observation. The linear trend estimation is derived by applying a least-squares fit analysis to the residuals, subtracting the model from the observation. Except for the daytime foF2, all the other parameters like nighttime foF2, day and nighttime h'F, and hmF2 show a negative trend. Present results suggest that the greenhouse effect is a prime driver for the observed long-term trend in the F-region. Interestingly, weak negative trends in the foE and foEs are found which contradicts an earlier investigation. The present study suggests that the changes in the upper stratospheric ozone and mesosphere wind shear variability could be the main driver for the observed weak negative trends in the foE, and foEs, respectively.

Plain Language Summary

Studies on the long-term trend are essential for understanding and quantifying the climate change impact on the Earth's atmosphere if it exist. In this investigation, we used fifty-six years of ionosonde measured E- and F-region parameters for a long-term trend estimation. We found a negative trend in the F-region ionospheric peak critical frequency (foF2), virtual height (h'F), and peak altitude (hmF2). More importantly, the nighttime trend is stronger than for the daytime. In particular, the daytime foF2 trend is statistically insignificant during this period. This suggests that the greenhouse effect and lower atmospheric forcing could have a predominant role in the observed trend in the F-region. In addition, E-region critical frequency and sporadic E-layer frequency also show a weak negative trend that could be due to the increasing trend in the northern hemisphere mid-latitude upper stratospheric ozone.

1 Introduction

The long-term trend is one of the challenging and debatable research topics because of the estimation method and the social relevance in the climate change scenario. Studies on the long-term changes in the upper atmosphere yield more attention after Roble and Dickinson (1989). Using a model simulation, they reported that due to the doubling of the CO_2 and CH_4 mixing ratios in the mesosphere and thermosphere, temperatures of these regions will cool about 10K and 50K, respectively. Motivated by the above investigation Rishbeth (1990) predicted that the greenhouse effect in the ionosphere under the composition changes and cooling mentioned by Roble and Dickinson (1989), the E- and F-region peak heights lower by about 2 km and 20 km, respectively, however, changes in the electron number density is very small. That study also postulated that a decrease in atmospheric pressure due to the cooling of the stratosphere, mesosphere, and thermosphere caused by the greenhouse effect is responsible for the descent in the ionospheric peak altitudes. At the same time a compensation of effects due to atmospheric composition and temperature changes could inhibit the changes in the plasma density. Using more than 30 years of ionosonde data, Bremer (1992) studied the ionospheric trends in the mid-latitudes, and his results were qualitatively in good agreement with Rishbeth (1990). Since then, there have been many investigations which looked into the seasonal,

latitudinal, and longitudinal variation of the long-term trends in the E- and F-region ionosphere (Bremer et al., 2004; Bremer & Peters, 2008; Bremer, 2008; A. Danilov, 2008, 2009, 2015; Danilov & Konstantinova, 2020; Laštovička et al., 2008; Laštovička et al., 2012; Laštovička, 2017, 2022; Mielich & Bremer, 2013; Mikhailov & Marin, 2001; Mikhailov & de la Morena, 2003; Mikhailov, 2006; Prasad et al., 2012). The outcome of these investigations shows that the long-term trend in the foF2 and hmF2 is not uniform, for example, in some of these locations the trend is positive and some other stations show a negative trend (Bremer et al., 2004; Mielich & Bremer, 2013). Most of these studies have postulated that the greenhouse effect is a prime cause of the observed trends (Bremer & Peters, 2008; Laštovička et al., 2012). In contradiction, Mikhailov and Marin (2001) suggest that the observed trends associated with the geomagnetic activity variations i.e. are of natural origin. However, lately using whole atmosphere model simulations Qian et al. (2021) found that trends in the thermosphere were predominantly driven by greenhouse gases, whereas in the foF2, hmF2 and Te the role of greenhouse gases and of the secular change of the geomagnetic field were comparable in some regions. However, globally the role of magnetic field change is negligible because locally it is both positive and negative.

Recently, Cnossen (2020) studied the long-term trend in the upper atmospheric neutral temperature, neutral density at 400 km altitude, and hmF2, NmF2 as well as TEC using the Whole Atmosphere Community Climate Model eXtension (WACCM-X) simulation data from 1950 to 2015. The authors found a negative trend in all these parameters and argued that CO_2 is probably the main driver of trends in the thermosphere. However for high (magnetic) latitudes, effects of changes in the Earth's magnetic field also appear to be important. Main magnetic field changes are likely responsible for a long-term decrease in Joule heating, which is especially important at low/equatorial latitudes of American sector. Her simulation also showed that trends associated with main magnetic field changes can be either positive or negative, depending on the location, patches of negative trends are considerably stronger and larger than patches of positive trends because main magnetic field changes push global mean trends to be more negative than they would be due to the increase in CO_2 concentration alone. In a nutshell, several factors may contribute to the long-term changes and trends in the upper atmosphere [Laštovička et al. (2012)], namely stratospheric ozone depletion, long-term changes in solar and geomagnetic activity, secular changes in the Earth's magnetic field, long-term changes of atmospheric circulation and atmospheric wave activity, and of mesospheric water vapor concentration. However, one of the prime factors of long-term changes and trends in the foF2 is CO_2 (Laštovička, 2022).

Most of the earlier investigations mainly studied the long-term trends in the F and/or E region critical frequencies, and peak altitudes (Bremer & Peters, 2008; Mikhailov, 2006). In the case of sporadic E layers, most of the earlier studies focused on the occurrence characteristics, seasonal and solar activity dependency, but very few reports are available on the long-term trends in foEs (Abdu et al., 1996; Pezzopane et al., 2015). In the present investigation, we used 63 years of continuous ionosonde data to estimate the long-term variations in the daytime E region parameters, namely foE, foEs, and day and nighttime F-region parameters such as h'F, hmF2, and foF2, and 56 years of data for the trends estimation of the above parameters over Juliusruh, Germany. Instrumentation and methodology are provided in section 2, and results and discussion are given in sections 3 and 4, respectively. Finally, section 5 describes the concluding remarks.

2 Instrumentation and method

We study the long-term variations and trends in the E- and F-region using an ionosonde observation over Juliusruh (54.6°N, 13.4°E) representing a high-mid latitude transition region in northern Germany. Long period oscillations and trends are investigated using

Lomb Scargle Periodogram (LSP), and least-square fitting analysis, respectively. A detailed description of the ionosonde and the methodology are given below.

2.1 Ionosonde

The ionosonde over Juliursh provides one of the longest, and most continuous observations around the globe and the data are available since July 1957. Thus, in total sixty-three years of data are available as of 2020, which are used for the estimation of long-term variations. However, to avoid any artificial negative slope due to the starting year 1957 (solar maximum) and the end year 2020 (solar minimum), only 56 years of data are used to investigate the long-term trends. Therefore, we consider only the years between 1964 to 2019 (both are the solar-minimum years) for the trend estimation. At first, we estimate the hourly median of E- and F-region ionospheric parameters such as h'F, h'Es, foE,foEs, h'F, foF2, hmF1 and hmF2. Then, the monthly median of hourly data is calculated, followed by the daytime and nighttime mean values are estimated by averaging the data during the time interval of 08-14 UT and 21-01 UT, respectively (centered around 11 and 23 UT). Note here that the virtual height h'F is directly observed from the ionograms. However, hmF1 and hmF2 are the real heights which are estimated using the Shimazaki's formula as described by Mielich and Bremer (2013). The following technical issues influence the monthly median data and have to be noticed to understand a possible exclusion of some periods or characteristics from the analyzed data set:

a) Until 1990 a high-power ionosonde with a starting frequency of ∼500 kHz was in operation. This allowed a recording of nighttime E layer critical frequencies but led to scaling of relatively high virtual E layer heights.

b) Between 1990 and 1994, a polish ionosonde of type KOS was in operation.

c) The high and not all the time stable output power of the first Juliusruh ionosondes influenced signal power-sensitive characteristics, like fmin and fbEs.

d) Since 1994, so-called Digisondes are in operation. From April to August 1998, during the upgrade from Digisonde model DPS-1 to DPS-4, an FMCW Barry Research Chirp Sounder was the replacement. With 3 km distance, the co-located Chirp Sounder receiver was too close to the transmitter to identify the ionospheric reflection in the presence of the ground wave in the ionogram. Daytime frequencies below ∼5 MHz, particularly h'E, foE, h'Es, foEs and fbEs were affected.

e) The formerly more intensely used commercial MF radio band up to 1.6 MHz led to partly strong interference and/or gaps in the ionograms, which made the scaling more difficult or impossible. In the modern Digisondes, the automatic RFIM algorithm may lead to gaps in the ionogram trace in that frequency range.

f) Former ionosondes were not able to distinguish between near vertical and oblique echoes and showed not only vertical but also some partly strong oblique echoes, which were scaled as vertical ones with relatively high virtual heights and with artificially higher values of foEs (Laštovička et al., 2012). Generally oblique echoes are mainly problem of Es due to their cloudy horizontal structure.

g) Modern national and international frequency regulations do not allow continuous transmitting over the whole frequency band. A specified restricted frequency list leads to several gaps of some 50kHz, which affects characteristics close to these restricted frequency bands.

h) Until 1992, different human scalers did the manual scaling of Juliusruh ionograms. After 1993, only one scaler was involved in that task until today. Even, when the manual scaling is done according to the official ionogram scaling rules, each human scaler tends to scale a bit to higher or lower values.

i) Juliusruh monthly medians are processed including the so-called qualitative and descriptive letters. Qualitative letters give information about the uncertainty of the value of up to 20%. In the long-term analysis of this paper, these letters remain unused.

While analyzing the data, we carefully removed the instrumental biases in the data set. For example to avoid errors in the trend estimation due to the instrumental capability we consider the foE only above 1MHz because before the 1980's the measurable lower frequency of ionosonde is 0.5 MHz after that it is changed to 1 MHz. It is worth to mention here that among historical ionosonde data from Europe the Juliusruh data are those of the best quality (Burešová, 1997).

2.2 Lomb Scargle Periodogram and Trend Analysis

It is essential to remove the short and long-period oscillations before the estimation of the linear trend (Laštovička et al., 2006; Laštovička & Jelínek, 2019). In literature, various solar proxies are used to remove the solar and geomagnetic influences on trend estimation. For example, Ap index, sunspot number, f10.7, E10.7, and so on. Recently, Lastovicka (2019); Laštovička (2021) showed that the optimum solar proxies are different for different ionospheric parameters. However, none of these studies removed the annual oscillations. Therefore, instead of using these proxies, we use a different approach to remove the solar cycle impact on the long-term trend estimation. As a first step, we use the Lomb Scargle Periodogram (LSP) analysis to identify the long-period oscillations and a Gaussian model fit. In the second step, using the period and amplitude of the long period oscillations and the Gaussian model parameters, a model ionosonde parameters X_m are constructed using the following equation.

$$X_m = Gaussian\ model(t) + A \cdot \sin(\frac{2\pi}{P_i})t + B \cdot \cos(\frac{2\pi}{P_i})t \quad (1)$$

$$Lt = X_{ob} - X_m \quad (2)$$

In the above equations, X_m and X_{ob} are modeled and observed ionosonde parameters, respectively. A, B, and P_i are the amplitude and period of the i^{th} oscillations (e.g., semi-annual and annual oscillation), respectively, and t is the time series of the data. In general, the above approach has been used to estimate the trends in the middle and lower atmosphere (Holmen et al., 2016). Since the solar cycle with its period of ∼9-12 years is one of the predominant oscillations in the data, we use a Gaussian model for better model data construction. The residual values are calculated by subtracting the model values from the observations, followed by the least-square fit analysis used to estimate the slope of the residual values or linear trend for the ionosonde parameters, namely foE, foEs, h'F, hmF2, and foF2.

3 Observations and results

3.1 Seasonal and diurnal variation of E- and F-region ionosonde parameters

To understand the seasonal and diurnal behavior, a climatology with 63 years of hourly parameter values of the E regions (i.e. foEs, foE, h'Es, h'E), are shown in Figures 1a-d. The critical frequencies foEs and foE show a diurnal variation of maxima and minima during the day and nighttime, respectively. They also exhibit seasonal variations with a maximum in local summer and a minimum during winter. The magnitude of foEs shows a wide/broad maximum peaking around local noon and increasing again towards ∼15:00 UT (see Fig. 1b). The foE peaks around local noon all the month. Please note that official local time over Juliusruh is universal time+2 (UT+2) and UT+1 hour during summer and winter, respectively. The diurnal variation of h'Es displays two prominent peaks viz., early morning and evening hours from March to September and only in around noon from October to February. The h'E shows two peaks viz., morning and in

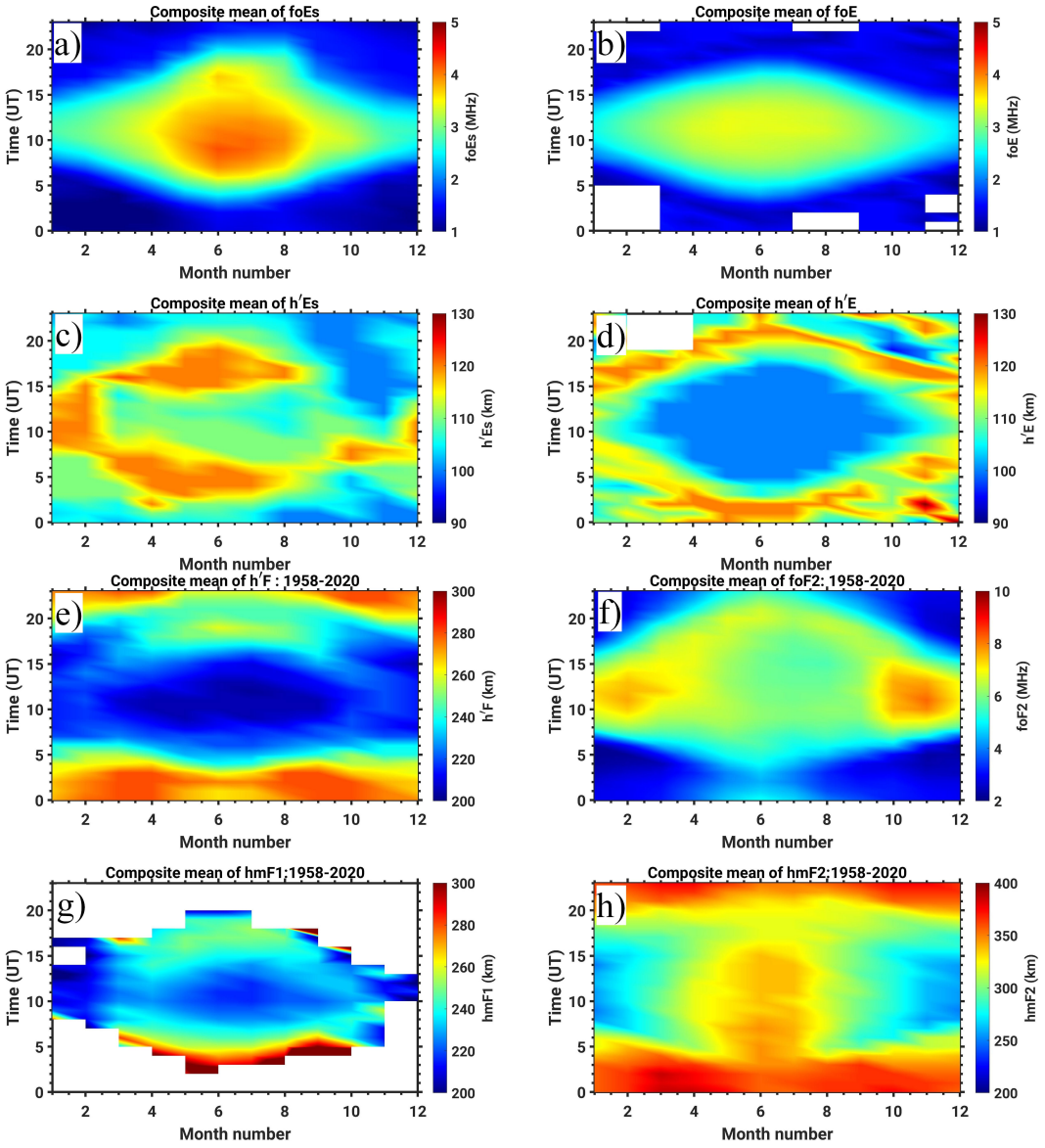

Figure 1. Diurnal and seasonal variation of composite mean of the 63 years of hourly median E (a-d), and F (e-h) region ionosonde parameters.

the evening hours along the year. Moreover, the h'E also show seasonal variation; summer and winter peaks occur in quite different times (see Fig.1a).

We also studied the seasonal and diurnal behavior, a climatology with 63 years of hourly parameter values of the F-regions (i.e. h'F, foF2, hmF1, and hmF2) are shown in Figure 1e-h. As expected, the virtual and real heights (h'F and hmF2) are generally lower during daytime, (especially for h'F) than in the nighttime. The hmF1 is only present in the daytime, particularly during the equinox and summer months. Most frequently, hmF2 is located around 350 km during nighttime, and the lowest altitudes of the hmF2 are observed in the winter daytime (∼250 km). On the other hand, the foF2 is higher in the winter than in the summer, which coincides with occurring at the lower altitudes. The foF2 show two peaks during summer, one is before noon, and the other is around 20 UT.

3.2 Monthly and inter-annual variation of the E- and F-region ionosonde parameters

Figure 2 shows the monthly median of hourly median E- and F-region ionosonde parameters, namely h'E, h'Es, foE, and foEs, from July 1957 to December 2020. The h'E data is available only during the daytime as described in the previous section, and does not show any diurnal variation. The distribution of h'Es shows morning and evening time enhancements in all the years, irrespective of height variations before and after 1990. Both the h'E and h'Es did not show any solar cycle variation. An important point to be noted here is this high differences in h'E, and h'Es altitudes before and after 1990 (see Fig.2a-b). These differences are implications of a high-power ionosonde with a starting frequency of ∼500 kHz, which was in operation until 1990. This characteristic allowed a recording of nighttime E layer critical frequencies but led to scaling of relatively high virtual E layer heights (as mentioned in Section 2.1). Due to these differences, the trend analysis was not perform from these parameters. The magnitude of the foE and foEs show an annual and solar cycle variation as shown in Figure 2c-d, and are higher during high solar activity than during lower solar activity years, as it is depicted in Figure 3c. Eventually, during the nighttime echoes from the E region altitudes are not observed for the used frequency range of above 1 MHz.

The diurnal and monthly variations of the h'F are shown in Figure 2e. The h'F is below and above 250 km during the day and nighttime in all the months, respectively. The h'F is very low i.e. below 200 km in the daytime of the solar minima years of the last three solar cycles. During the day and nighttime, h'F shows a clear solar cycle variation with higher altitudes during the high solar activity years. Figure 2f shows the diurnal and monthly variations of critical plasma frequency of the F2 (foF2). The foF2 is much higher during the daytime than nighttime, and the highest frequencies are observed around the local noon. Similarly, the foF2 is higher during the solar maxima years of the solar cycles 19, 21, 22, and 23 than the weaker solar cycles 20 and 24. Diurnal and monthly variations of the hmF1 and hmF2 are shown in Figures 2g and h, respectively. The hmF1 altitude is below and above 225 km during solar minima and maxima, respectively, and the echoes from the hmF1 layer is absent during the nighttime irrespective of the solar condition. In the case of hmF2, most often it is below 350 km during daytime and above 350 km at nighttime. The hmF2 maximum altitudes are located above 400 km during the nighttime of the solar maxima years of the solar cycles 19, 21, and 22.

The annual mean of the E- and F-region parameters viz. foF2 h'F, hmF2, foE and foEs are shown in Figures 3a-c to understand the year-to-year and solar cycle variations. In the F-region, foF2 and hmF2 show a strong positive correlation with sunspot number. However, in h'F, the solar cycle dependency is positive but rather feeble. In the E region, foE and foEs display a strong positive correlation till the 23rd solar cycle but weak during the 24th solar cycle. In particular, foEs at the solar minimum year 2008 is higher than at the solar maximum year 2014 (see Fig. 3c).

3.3 Long-term variations and residual trends

For the residual trend analysis we need to perform the LSP analysis to identify the predominant long-period oscillations and their amplitudes for each parameter. Using these periods and amplitude of the estimated oscillations model data are constructed using Equation 1. Obtained long-term variations and trends in the ionosonde parameters are detailed in the following subsections.

3.3.1 Long-term variations and residual trends in daytime foE and foEs

Daytime averaged monthly median of foE and foEs and their corresponding Lomb-Scargle periodogram are shown in Figures 4a-d. The overall, daytime mean of foE and

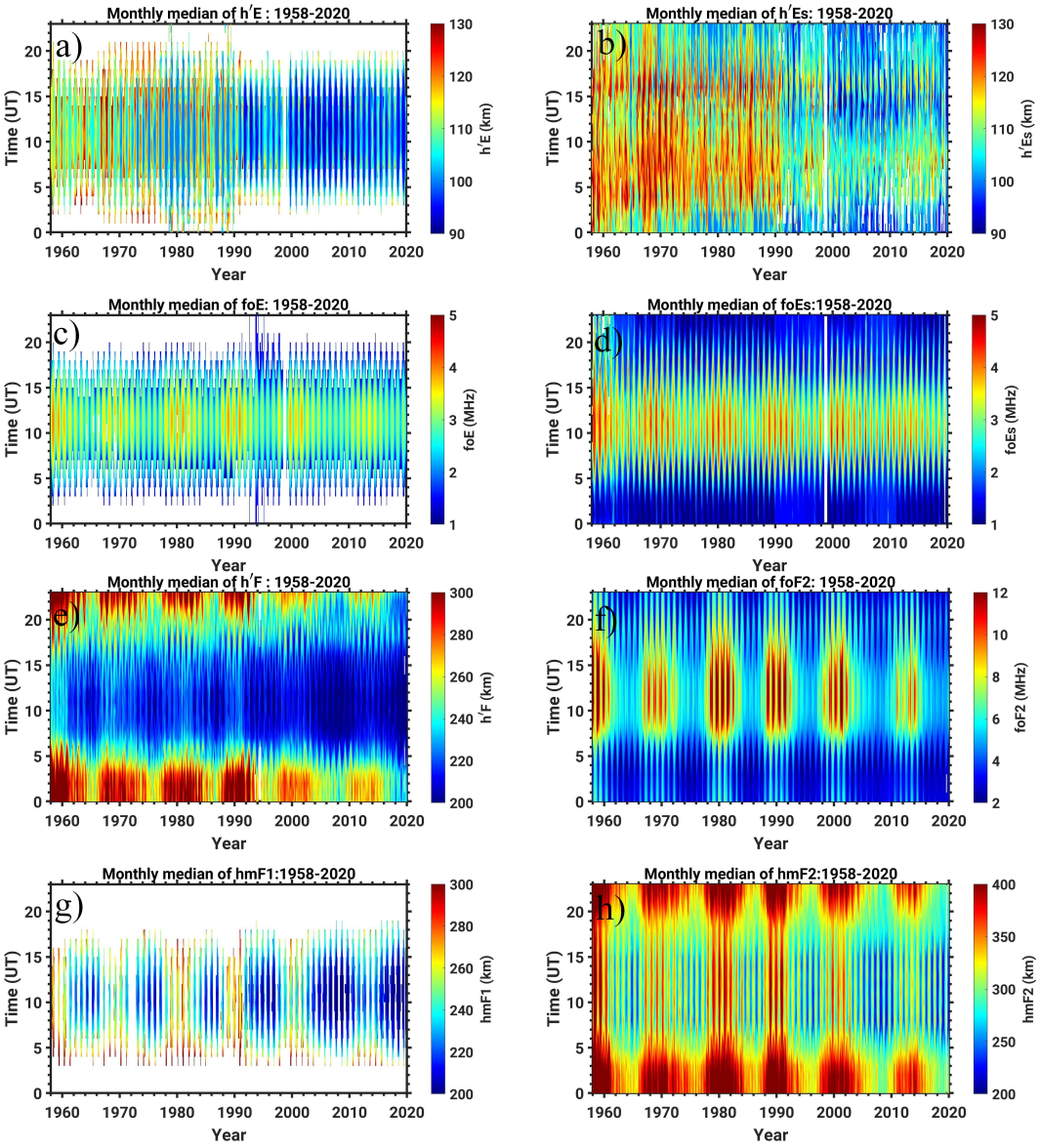

Figure 2. Diurnal variation of monthly mean of hourly median E (a-d), and F (e-h) region ionosonde parameters

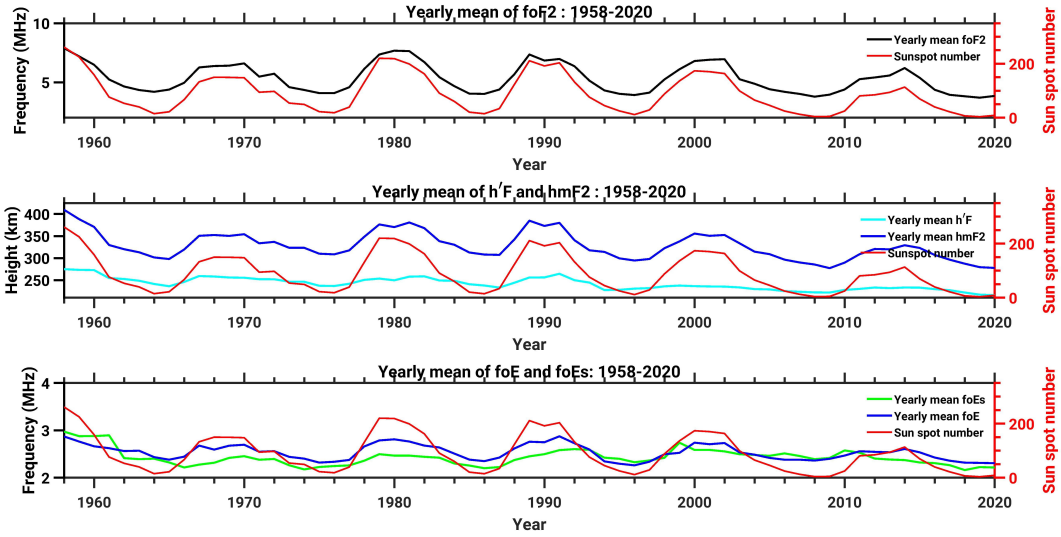

Figure 3. (a) Comparison of annual mean of foF2 and sunspot number, (b) hmF2 and h'F and sunspot number, and (c) foEs and foE and sunspot number.

foEs is 3.0±0.5 MHz and 3.2±0.6 MHz, respectively. The analysis shows that both of these parameters' annual oscillation is predominant in the E-region followed by the 11 years solar cycle variation also contributing to the long-term variations. Since the 11 years of the solar cycle shows a Gaussian-like structure, a 7th order Gaussian fitting is applied to the daytime averaged data, width, and amplitude of each solar cycle oscillation extracted. Combining the Gaussian fitted parameters, and LSP estimated period and amplitude of the other oscillation (e.g., annual oscillation), a model data is constructed using Equation 1 (detailed in Section 2). A similar analysis is carried out in all other parameters, which are detailed in the following subsections. A comparison of the observation and model estimated foE and foEs from 1958 to 2020 and shown in Figures 4e and g, it is obvious that both are in good agreement with each other. Furthermore, the model values are subtracted from the observational values to deduce the residual variations. By applying the least-square fit on the residual variation the linear slope is estimated and shown in Figures 4f and h. As mentioned in Section 2, to avoid the extremes of solar activity at the rim of time series, the high (the year 1958) and minimum (the year 2019) solar activity effect in the linear slope estimation, we considered only the years from 1964 to 2020 as both these years fall under the low solar activity condition. The foE and foEs show a weak negative slope of -0.7±0.59 kHz/yr (±0.59 represents 95% confidence interval) and -1.06±0.56 kHz/yr, respectively. The magnitude of the linear slopes are above the 95% confidence interval. Thus, it is reasonable to assume that the obtained negative trends in the slopes are outcomes of geophysical variation rather than an error or artifact.

3.3.2 Long-term variations and residual trends in day and nighttime foF2

The monthly medians of day and nighttime averaged foF2 are shown in Figures 5a and 5c, and their corresponding LSP analysis is shown in Figures 5b and 5d, respectively. The 63 years mean of a day and nighttime foF2 is ∼7±2 MHz and ∼4±1 MHz, respectively. From figures 5b and 5d, a distinct feature is observed that during the daytime the amplitude of the 11-year solar cycle variation is more predominant than the annual oscillation. In contrast, the amplitude of the annual oscillation is comparable to or larger than the 11-year solar cycle variation at nighttime. Figures 5e and 5g display the com-

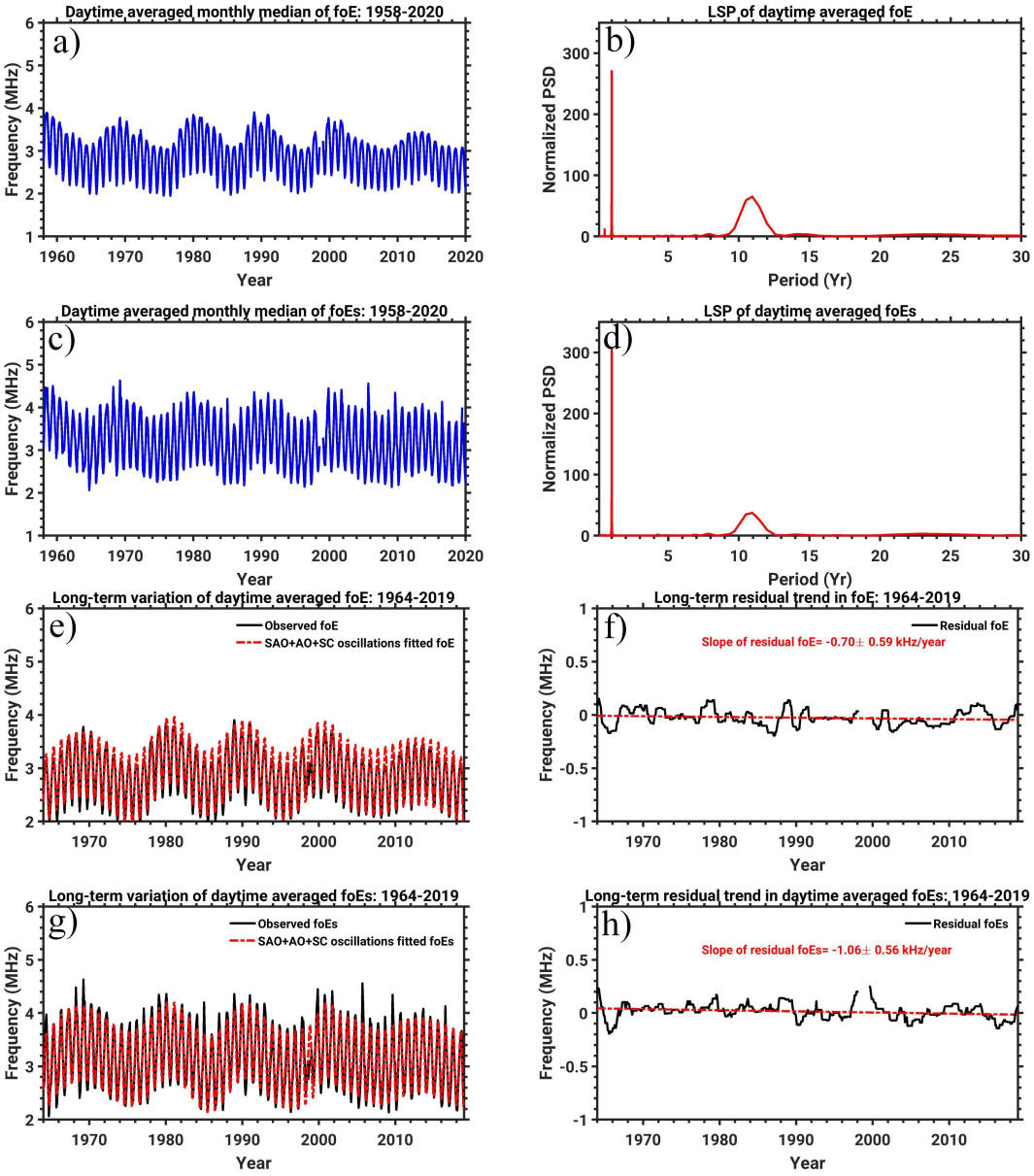

Figure 4. (a & c) Daytime averaged monthly median of foE and foEs and their LSP analysis (b & d), respectively. (e & g) Comparison of observation and model foE and foEs, (f & h) residual (black curve) of the foE and foEs and their linear trends (red dotted line)

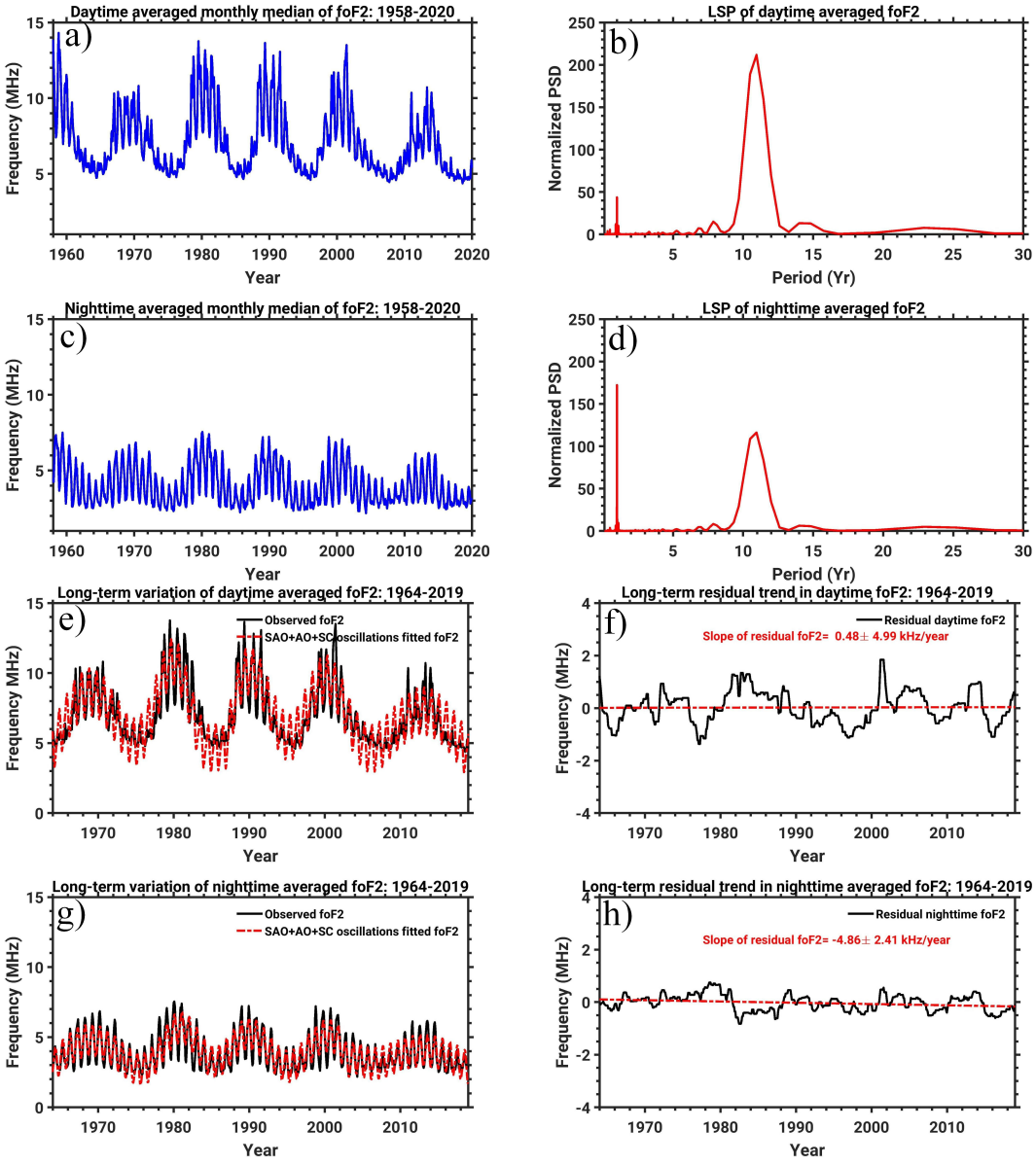

Figure 5. Same as Figure 4 but for day and nighttime foF2.

parison of observed and modeled foF2 values, during the low solar activity years the daytime modeled foF2, and in high solar activity years, the nighttime foF2 values are slightly underestimated. However, overall, the long-term variation of the observed and modeled values are showing good consistency. The residual values are estimated by subtracting the model values from the observation, which is shown in Figures 5f and 5h (black curve), in these figures the slope of the least-squares fit is also shown (red dotted line). Interestingly, the daytime foF2 shows a very weak positive slope of 0.48±5 kHz/yr, however, the estimated slope is statistically quite insignificant. On the other hand, during the nighttime, a clear negative trend in the slope is observed with ∼-5±2.4 kHz/yr.

3.3.3 Long-term variations and residual trends in day and nighttime h'F

Figures 6a and 6c represent the day and nighttime averaged monthly median of h'F, and their corresponding LSP are given in Figures 6b and 6d. The 63 years' mean virtual altitude of the day and nighttime h'F is located around 213±11 km and 270±22 km, respectively. As expected during the nighttime the bottom of the F layer height is higher than during the daytime. Note, also that the measured nighttime h'F values are slightly overestimated due to he lower limit of sounding frequency. Contrary to the foF2, the ∼11-year solar cycle variation is the primary contributor to the long-term variation irrespective of day and night, followed by a weak annual and semi-annual periodicity is also exists. Using these periods and amplitudes model values are constructed, and the comparison of model and observation is given in Figures 6e and 6g both are matching quite well. The residual h'F for the day and nighttime is estimated by subtracting the model values from the observation, which is shown in Figures 6f and 6h. The linear residual slope is negative for both day and night with ∼-50±33 m/yr and ∼-72±72 m/yr.

3.3.4 Long-term variations and residual trends in day and nighttime hmF2

Figure 7a-d show the day and nighttime averaged monthly median of hmF2 and their corresponding LSP analysis. The mean altitude of the day and nighttime hmF2 is found at 303±43 km and 363±41 km, respectively. Similar to the h'F, hmF2 also shows the nighttime F2 peak altitude is higher than the daytime. Another interesting observation is that the annual oscillation is more predominant than the 11-year solar cycle variation during daytime, where for the nighttime hmF2 basically only the 11 years solar cycle is visible. The observation and model hmF2 values are remarkably in agreement with each other which is shown in Figures 7e and 7g. The linear residual slope is negative for both day and nighttime with the magnitude of -54 ±115 m/yr and -240 ±110 m/yr, however for the daytime the estimated slope is below the 95% confidence interval. From these results, it is clear that the ionospheric peak height shows a descending tendency. Moreover, the rate of descending is stronger during the night than in the daytime. Another important point is that during daytime the decreasing tendency in the h'F and hmF2 are nearly comparable, however nighttime decreasing trend in hmF2 is 3 times larger than that in h'F. Overall, day and nighttime E- and F-region linear residual trends estimated in the present study are given in Table 1.

Table 1. Linear residual trends in E- and F-region parameters

Region	Parameter	Daytime	Nighttime
E	foE	-0.7 ± 0.6 kHz/yr	NIL
	foEs	-1.1 ± 0.6 kHz/yr	NIL
F	foF2	0.5 ± 5 kHz/yr	-5 ± 2.4 kHz/yr
	h'F	-50 ± 33 m/yr	-72 ± 72 m/yr
	hmF2	-54 ± 116 m/yr	-240 ± 110 m/yr

4 Discussion

In the present study, we used a new approach to estimate the long-term variations and linear residual trends, which will help to better understand their behavior in the E- and F-region over Juliusruh, Germany.

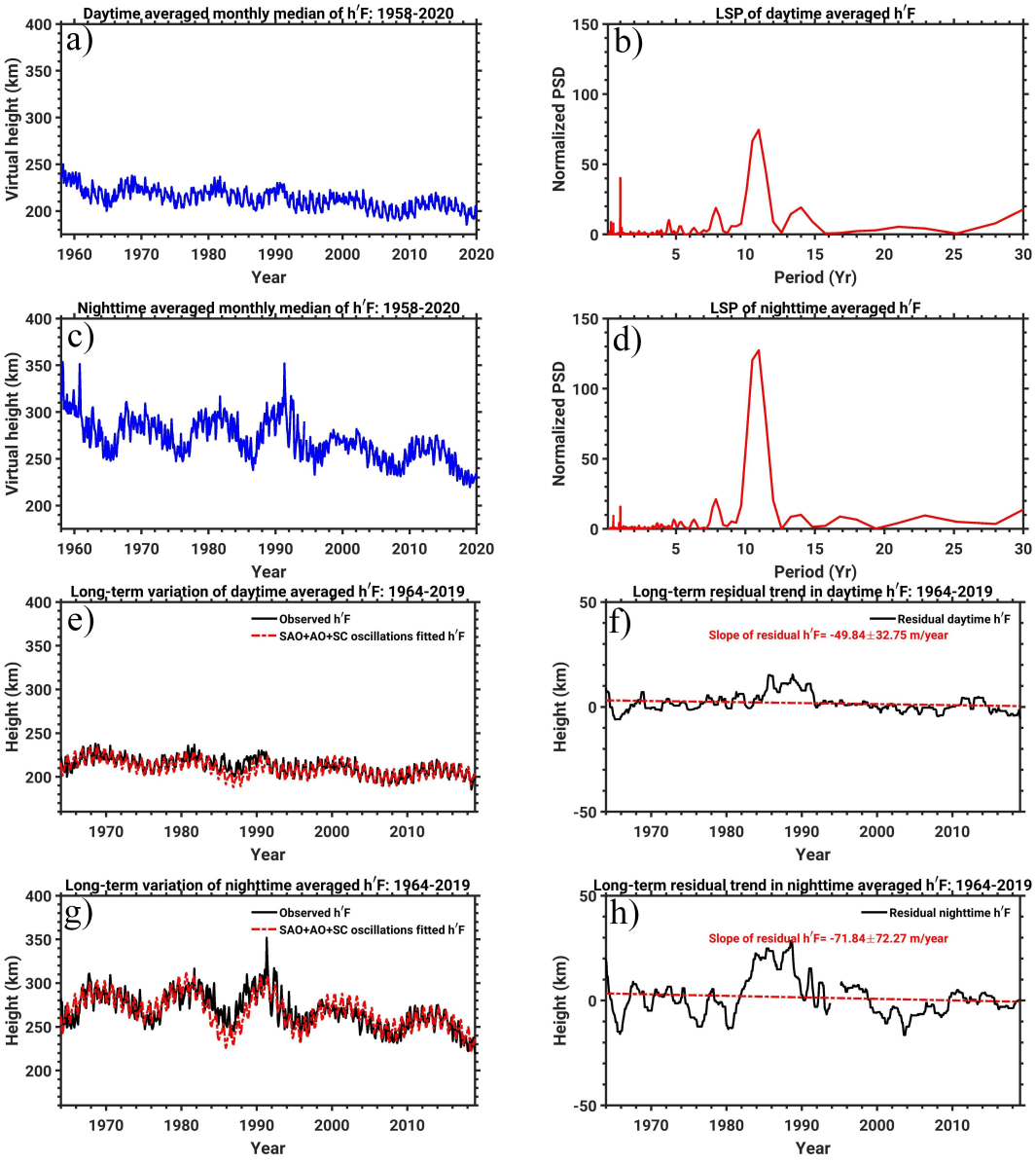

Figure 6. Same as Figure 4 but for day and nighttime h'F.

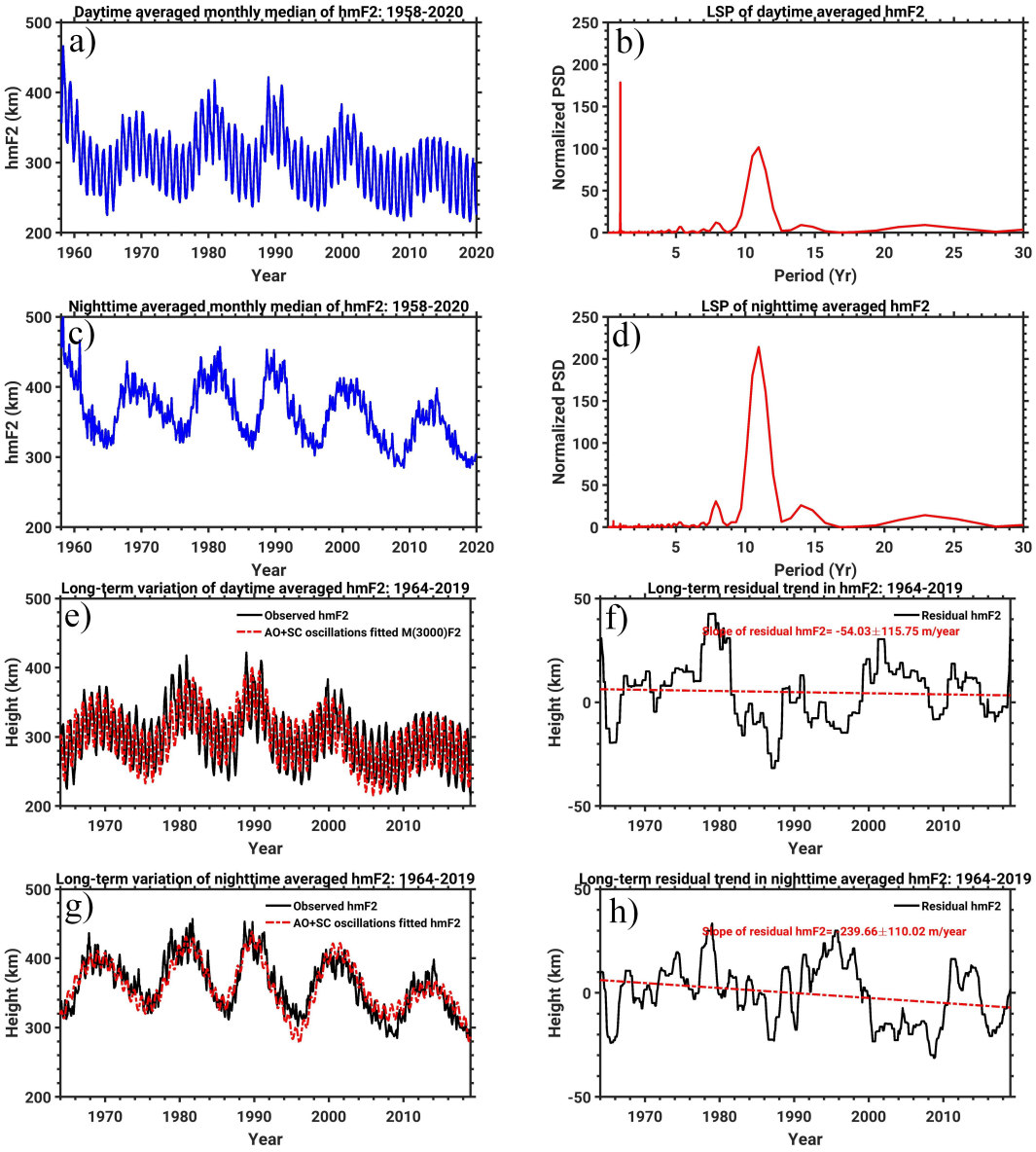

Figure 7. Same as Figure 4 but for day and nighttime hmF2

In the F-region, it is expected that the 11-year solar cycle variation is the prime driver for long-term oscillation. However, the day and nighttime shows a different picture, for example, for daytime hmF2 and nighttime foF2, the amplitude of the annual oscillation is comparable to or higher than the 11-year solar cycle oscillation. This suggests that while using the foF2 and hmF2 monthly median data for the long-term trend estimations, in addition to the solar cycle variation annual oscillation is also to be removed. Using the Global Ultraviolet Imager (GUVI) onboard the Thermosphere Ionosphere Mesosphere Energetics and Dynamics (TIMED) satellite data, Yue et al. (2019) reported that the annual oscillation in O and O/N2 number density ratio is strong in mid-latitudes. On fixed pressure levels, O and N2 densities are anticorrelated with solar extreme ultraviolet fluxes in the upper thermosphere. On the other hand, O/N2 is smaller during solar minimum and larger during solar maximum. Thus, we suggest that changes in composition and neutral atmospheric dynamics could cause the observed strong annual oscillations in the nighttime foF2 and daytime hmF2. In the E-region, the critical frequencies namely, foE and foEs depict robust annual and weak 11-year solar cycle oscillations. These oscillations could be caused by seasonal and long-term variations of solar heating.

We found that except for daytime foF2, all the other parameters in the F-region show a negative trend in both day and nighttime. Both the day and nighttime the linear residual slope values are almost similar for h'F. Interestingly for foF2 and hmF2, the nighttime linear residual trend is stronger than the daytime. Moreover, the nighttime hmF2 trend (i.e.-240 m/yr) is in good agreement with a previous investigation by Bremer (1992), in which the author used 33 years of ionosonde data. However, the present trend in the foF2 is twice the magnitude of Bremer's estimation. One plausible reason could be that over the year the peak altitude of the F-region has declined linearly. On the other hand, the negative trend in the peak frequency is increasing rapidly compared to the earlier times. However, during the daytime foF2 linear residual slope is almost none, quite insignificant. In daytime hmF2, the linear residual slope value is four times lesser than the nighttime trend. The estimated linear residual slope of h'F and hmF2 are nearly the same in the daytime, but the residual slope of h'F is four times smaller than the hmF2 in the nighttime. Moreover, the daytime residual slope in the foF2 and hmF2 are statistically insignificant (see Table 1). Note, that the measured nighttime h'F values are slightly overestimated due to he lower limit of sounding frequency. One probable reason for the noted difference between nighttime h'F and hmF2 could be the observational limitation of the h'F due to the electron density reduction in the bottom of the ionosphere.

At daytime, due to the interaction of chemical loss, plasma diffusion, and neutral winds, the height of the E- and F-layer peaks corresponds to a fixed pressure level in the neutral atmosphere. Whereas at nighttime, the E-layer is weak and not observable by ionosonde, and the dynamical processes such as neutral winds and electric fields drive the F2-layer (Rishbeth & Edwards, 1989). Under the steady-state assumption, a $\sim$50K decrease in temperature could lower the ionospheric peak altitude (hmF2) by 15 and 20 km at noon and midnight, respectively (Rishbeth, 1990). That is a nearly 3:4 ratio of decrement in peak altitude between day and nighttime at a uniform day and nighttime cooling. According to the present results in the last 56 years, the hmF2 lowered by 13.4 (240m/yr) and 3 km (50m/yr) during night and daytime, respectively. The decreasing tendency is in good agreement with Rishbeth (1990), however, the descending ratio between day and nighttime shows a large discrepancy (1:4). In addition to the CO2 cooling, secular changes in the geomagnetic activity are also proposed as a driver for the long-term trend in the F2-layer. During the period of 1965 to 2020, according to the IGRF (International Geomagnetic Reference Field) model the geomagnetic latitude changed from 54.31°N in 1965 to 54.14°N, implicating negligible effect in Juliusruh. However, the geomagnetic variations are highly regional dependent that could not explain the noted day and nighttime differences. This arises the question of why the decreasing trend or ionospheric response to the cooling effect during the day and nighttime is different?

Rishbeth (1990) postulated that the global cooling may not have any significant impact on daytime critical frequency foF2, because the cooling will increase the O/N2 that will cause an increase in the plasma density. On the other hand, the loss coefficient also will increase that causes to decrease the plasma density, combination of these two effects will cancel out each other. In the present case, daytime foF2 shows a statistically insignificant positive trend that is consistent with the greenhouse effect. However, using three ionosonde stations over Europe (including Juliusruh), A. Danilov (2015) reported a negative trend with a maximum during the daytime and a minimum at nighttime. The author also argued that the decreasing trend in the neutral temperature did not cause the observed negative trend, instead, a systematic decrease in the atomic oxygen concentration in the thermosphere could be a probable driver of the negative trend in the foF2. Furthermore, using model simulations Qian et al. (2009) also showed a negative and positive trend in the day, and nighttime foF2 respectively, for which they argued the greenhouse effect is the prime driver, and meridional neutral wind dynamics also have a significant role. In contradiction with the earlier investigations, we found a stronger negative trend at nighttime and a very weak positive or zero slope during daytime. Considering the trend pattern, we believe that the thermospheric cooling and composition changes driven by the green house effect could be balanced by the insolation driven heating and ionisation in daytime. On the other hand, during the nighttime in the absence of sunlight green house effect associated changes in the composition might cause the estimated negative trend in foF2 over Juliusruh.

Since the nighttime E-layer is weak and not observable by ionosonde, we estimate only the daytime linear residual trend in the foE and foEs. Earlier, Mikhailov (2006) reported a positive trend in foE, and similarly, Bremer and Peters (2008) also showed a positive trend in foE from 1957 to 2002, over Juliusruh. However, the present results show a negative trend in the foE. For the first time, we also report a negative trend in the daytime foEs over Juliusruh. Two potential drivers are proposed for the E region plasma density trends in literature, namely 1) decrease of NO in the E region heights (Mikhailov, 2006) and changes in the stratospheric ozone (Bremer & Peters, 2008). In addition, Mikhailov and de la Morena (2003) found foE trends to be geomagnetically controlled before about 1970. Followed by Laštovička (2005) reported that the role of solar and geomagnetic activity decreased from the beginning to the end of the 20th century. According to Bremer and Peters (2008), the foE trend is in anti-correlation with the O_3. A recent report by Petropavlovskikh et al. (2019) the SPARC-LOTUS (Stratosphere-Troposphere and their Role in climate-Long-term Ozone Trends and Uncertainties in the Stratosphere) showed that in the northern hemisphere upper stratosphere, the ozone concentration is increasing by 3-5%. Thus, it provides evidence that the increment in the upper stratospheric ozone could cause the decreasing trend of foE. Furthermore, we also agree that there also may be some contribution by the NO. We plan to study the long-term change in the mesospheric NO using model simulations in the future. E-region parameter trends are very weak and, therefore, very sensitive to various influences.

The wind shear theory is a well-recognized mechanism for the formation of the Es layer in the mid-latitudes (Mathews, 1998). According to the wind shear theory, ions with significant lifetimes against recombination are accumulated by the westward neutral winds above and eastward or weak westward wind below in the E-region. Studies also have suggested that in the midlatitudes, the Es-layer occurrence rate strongly depends on the combination of negative wind shears and sporadic meteor deposition in the upper atmosphere (Haldoupis et al., 2007). Furthermore, the wind shear in the mesosphere lower thermosphere is primarily driven by the tides, particularly semidiurnal, terdiurnal, and quarterdiurnal tides in the mid-latitudes, thus the Es layer occurrence also shows a semi-diurnal tidal pattern (Arras et al., 2009; Jacobi & Arras, 2019). A recent study using meteor radar wind observations shows a tendency of stronger eastward and southward directed winds during the last decade (Jacobi et al., 2015) for the mid-latitudes. Thus, we suggest that the weakening of the westward wind in the E-region altitude could suppress the ion ac-

cumulations as a consequence the wind shear could be a reason for the obtained negative trend in foEs. Besides, meteor deposition and tidal variability's role in the foEs negative trend is also worth investigating in the future.

5 Concluding remarks

The present study investigates the long-term variations and linear residual trends using sixty-three years of the E- and F-region ionosonde parameters: foE, foEs, h'F, foF2, and hmF2. The obtained results and their causes are listed below:

1. Using the LSP analysis the predominant oscillations in the E- and F-region ionosonde parameters are identified. Furthermore, the amplitudes and width of the solar cycle oscillation are estimated using a Gaussian model fit.

2. The present analysis exhibit that the annual and solar cycle oscillation has a significant role in the long-term variation in the critical plasma frequencies and altitudes of the F2-layer. The amplitude of the 11-year solar cycle oscillation is more dominant than the annual oscillation in the day and nighttime h'F, daytime foF2, and nighttime hmF2, and the amplitude of the annual oscillation is higher than the solar cycle in nighttime foF2 and daytime hmF2. On the other hand, the annual oscillation presides over the 11-year solar cycle oscillation in the daytime foE and foEs.

3. For the trend estimation, in addition to the solar and geomagnetic proxies, the annual oscillations also should be removed from the monthly mean data. In particular, the amplitude of the annual oscillation is stronger than the 11-year solar variation in the E-region. Thus, it can affect the trend estimation.

4. Using the period and amplitude of the predominant oscillations model values of foE and foEs, h'F, hmF2, and foF2 are constructed, and these model estimates are comparable with the observation. The residual values are estimated by subtracting the model values from the observation. Then, by applying the least-squares fit analysis long-term trends in the above parameters are calculated.

5. In the F-region, daytime averaged foF2 shows weak positive but quite insignificant trend of 0.5 kHz/yr, and during nighttime a negative trend of 5 kHz/yr. Day and nighttime averaged h'F show a weak negative trend of 50 m/yr and 72 m/yr, respectively. On the other hand, hmF2 shows a weak and strong negative trend of 54 m/yr and 240 m/yr during the day and nighttime, respectively. Overall, the hmF2 and foF2 nighttime trends are stronger than in the daytime. Our investigation suggests that the greenhouse effect is the prime driver for the daytime foF2 and day and nighttime hmF2 long-term trend. Furthermore, dynamics and composition changes also contributed to the negative trend in nighttime foF2.

6. We also found a weak negative trend in both foE and foEs of 0.7 kHz/yr and 1.06 kHz/yr, respectively, in the E region. We speculate that the increasing trend in the upper stratospheric ozone might be a prime factor for the decreasing trend in the E region critical frequency. Similarly, changes in the neutral wind shear might be a driving mechanism for the noted negative trends in foEs.

Acknowledgments
One of the authors, M. Sivakandan, acknowledges the financial support provided by the Alexander-von-Humboldt Foundation and the research opportunity provided by the Leibniz Institute of Atmospheric Physics (IAP). J.L. acknowledges support by the Czech Science Foundation under grant 18-01625S.

6 Data Availability Statement

The ionosonde data used in this study are openly available at `https://www.sws.bom.gov.au/World_Data_Centre/1/3`. The sunspot number data is available at `https://lasp.colorado.edu/lisird/data/american_relative_sunspot_number_daily/`

References

Abdu, M. A., Batista, I. S., Muralikrishna, P., & Sobral, J. H. (1996). Long term trends in sporadic E layers and electric fields over Fortaleza, Brazil. *Geophysical Research Letters*, *23*(7), 757–760. doi: 10.1029/96GL00589

Arras, C., Jacobi, C., & Wickert, J. (2009). Semidiurnal tidal signature in sporadic e occurrence rates derived from gps radio occultation measurements at higher midlatitudes. *Annales Geophysicae*, *27*(6), 2555–2563. Retrieved from `https://angeo.copernicus.org/articles/27/2555/2009/` doi: 10.5194/angeo-27-2555-2009

Bremer, J. (1992). Ionospheric trends in mid-latitudes as a possible indicator of the atmospheric greenhouse effect. *Journal of Atmospheric and Terrestrial Physics*, *54*(11), 1505-1511. doi: 10.1016/0021-9169(92)90157-G

Bremer, J. (2008). Long-term trends in the ionospheric e and F1 regions. *Annales Geophysicae*, *26*(5), 1189–1197. doi: 10.5194/angeo-26-1189-2008

Bremer, J., Alfonsi, L., Bencze, P., Laštovička, J., Mikhailov, A. V., & Rogers, N. (2004). Long-term trends in the ionosphere and upper atmosphere parameters. *Annals of Geophysics*, *47*, 1009–1029. doi: 10.4401/ag-3283

Bremer, J., & Peters, D. (2008). Influence of stratospheric ozone changes on long-term trends in the meso- and lower thermosphere. *Journal of Atmospheric and Solar-Terrestrial Physics*, *70*(11-12), 1473–1481. doi: 10.1016/j.jastp.2008.03.024

Burešová, D. (1997). Results of fof2 data testing with the undiv program. *Studia Geophysica et Geodaetica*, *41*(1), 82-87. doi: 10.1023/A:1023392808566

Cnossen, I. (2020). Analysis and Attribution of Climate Change in the Upper Atmosphere From 1950 to 2015 Simulated by WACCM-X. *Journal of Geophysical Research: Space Physics*, *125*(12). doi: 10.1029/2020JA028623

Danilov, & Konstantinova, A. V. (2020). Long-Term Variations in the Parameters of the Middle and Upper Atmosphere and Ionosphere (Review). *Geomagnetism and Aeronomy*, *60*(4), 397–420. doi: 10.1134/S0016793220040040

Danilov, A. (2008). Long-term trends in the relation between daytime and nighttime values of foF2. *Annales Geophysicae*, *26*(5), 1199–1206. doi: 10.5194/angeo-26-1199-2008

Danilov, A. (2009). Critical frequency foF2 as an indicator of trends in thermospheric dynamics. *Journal of Atmospheric and Solar-Terrestrial Physics*, *71*(13), 1430–1440. doi: 10.1016/j.jastp.2008.04.001

Danilov, A. (2015). Seasonal and diurnal variations in f o F 2 trends. *Journal of Geophysical Research: Space Physics*, *120*(5), 3868–3882. doi: 10.1002/2014JA020971

Haldoupis, C., Pancheva, D., Singer, W., Meek, C., & MacDougall, J. (2007). An explanation for the seasonal dependence of midlatitude sporadic E layers. *Journal of Geophysical Research: Space Physics*, *112*(6), 1–7. doi: 10.1029/2007JA012322

Holmen, S. E., Hall, C. M., & Tsutsumi, M. (2016). Neutral atmosphere temperature trends and variability at 90km, 70°N, 19°E, 2003-2014. *Atmospheric Chemistry and Physics*, *16*(12), 7853–7866. doi: 10.5194/acp-16-7853-2016

Jacobi, C., & Arras, C. (2019). Tidal wind shear observed by meteor radar and comparison with sporadic e occurrence rates based on gps radio occultation observations. *Advances in Radio Science*, *17*, 213–224. Re-

555 trieved from https://ars.copernicus.org/articles/17/213/2019/ doi:
556 10.5194/ars-17-213-2019
557 Jacobi, C., Lilienthal, F., Geißler, C., & Krug, A. (2015). Long-term variability
558 of mid-latitude mesosphere-lower thermosphere winds over Collm (51° N, 13°
559 E). *Journal of Atmospheric and Solar-Terrestrial Physics*, *136*, 174-186. doi:
560 10.1016/j.jastp.2015.05.006
561 Laštovička, J. (2017). A review of recent progress in trends in the upper atmo-
562 sphere. *Journal of Atmospheric and Solar-Terrestrial Physics*, *163*, 2–13. doi:
563 10.1016/j.jastp.2017.03.009
564 Lastovicka, J. (2019). Is the Relation Between Ionospheric Parameters and Solar
565 Proxies Stable? *Geophysical Research Letters*, *46*(24), 14208–14213. doi: 10
566 .1029/2019GL085033
567 Laštovička, J. (2021). What is the optimum solar proxy for long-term ionospheric in-
568 vestigations? *Advances in Space Research*, *67*(1), 2–8. doi: 10.1016/j.asr.2020
569 .07.025
570 Laštovička, J. (2022). Long-Term Changes in Ionospheric Climate in Terms of foF2.
571 *Atmosphere*, *13*(1). doi: 10.3390/atmos13010110
572 Laštovička, J., & Jelínek. (2019). Problems in calculating long-term trends in the
573 upper atmosphere. *Journal of Atmospheric and Solar-Terrestrial Physics*,
574 *189*(10), 80–86. doi: 10.1016/j.jastp.2019.04.011
575 Laštovička, J., Mikhailov, A. V., Ulich, T., Bremer, J., Elias, A. G., Ortiz de Adler,
576 N., ... Danilov, A. D. (2006). Long-term trends in foF2: A comparison of var-
577 ious methods. *Journal of Atmospheric and Solar-Terrestrial Physics*, *68*(17),
578 1854–1870. doi: 10.1016/j.jastp.2006.02.009
579 Laštovička, J., Solomon, S. C., & Qian, L. (2012). Trends in the neutral and ionized
580 upper atmosphere. *Space Science Reviews*, *168*(1-4), 113–145. doi: 10.1007/
581 s11214-011-9799-3
582 Laštovička, J. (2005). On the role of solar and geomagnetic activity in long-term
583 trends in the atmosphere–ionosphere system. *Journal of Atmospheric and*
584 *Solar-Terrestrial Physics*, *67*(1), 83-92. doi: 10.1016/j.jastp.2004.07.019
585 Laštovička, J., Akmaev, R. A., Beig, G., Bremer, J., Emmert, J. T., Jacobi, C.,
586 ... Ulich, T. (2008). Emerging pattern of global change in the upper at-
587 mosphere and ionosphere. *Annales Geophysicae*, *26*(5), 1255–1268. doi:
588 10.5194/angeo-26-1255-2008
589 Laštovička, J., Boška, J., Burešová, D., & Kouba, D. (2012). High historical val-
590 ues of foEs-reality or artefact? *Journal of Atmospheric and Solar-Terrestrial*
591 *Physics*, *74*, 51-54. doi: 10.1016/j.jastp.2011.10.008
592 Mathews, J. (1998). Sporadic E: current views and recent progress. *Journal of At-*
593 *mospheric and Solar-Terrestrial Physics*, *60*(4), 413–435. doi: 10.1016/S1364
594 -6826(97)00043-6
595 Mielich, J., & Bremer, J. (2013). Long-term trends in the ionospheric F2 region with
596 different solar activity indices. *Annales Geophysicae*, *31*(2), 291–303. doi: 10
597 .5194/angeo-31-291-2013
598 Mikhailov, A. V. (2006). Trends in the ionospheric E-region. *Physics and Chemistry*
599 *of the Earth*, *31*(1-3), 22–33. doi: 10.1016/j.pce.2005.02.005
600 Mikhailov, A. V., & de la Morena, B. A. (2003). Long-term trends of ¡i¿f¡/i¿oE and
601 geomagnetic activity variations. *Annales Geophysicae*, *21*(3), 751–760. doi: 10
602 .5194/angeo-21-751-2003
603 Mikhailov, A. V., & Marin, D. (2001). An interpretation of the foF2 and hmF2
604 long-term trends in the framework of the geomagnetic control concept. *Annales*
605 *Geophysicae*, *19*(7), 733–748. doi: 10.5194/angeo-19-733-2001
606 Petropavlovskikh, I., Hubert, D., Damadeo, R., Hassler, B., & Sofieva, V. (2019).
607 *SPARC/IO3C/GAW report on Long-term Ozone Trends and Uncertainties in*
608 *the Stratosphere* (Tech. Rep. No. 9).
609 Pezzopane, M., Pignalberi, A., & Pietrella, M. (2015). On the influence of solar

activity on the mid-latitude sporadic E layer. *Journal of Space Weather and Space Climate*, *5*. doi: 10.1051/swsc/2015031

Prasad, S. N., Prasad, D. S., Venkatesh, K., Niranjan, K., & Rama Rao, P. V. (2012). Diurnal and seasonal variations in sporadic E-layer (Es layer) occurrences over equatorial, low and mid latitude stations - a comparative study. *Indian Journal of Radio and Space Physics*, *41*(1), 26–38.

Qian, L., Burns, A. G., Solomon, S. C., & Roble, R. G. (2009). The effect of carbon dioxide cooling on trends in the F2-layer ionosphere. *Journal of Atmospheric and Solar-Terrestrial Physics*, *71*(14-15), 1592–1601. doi: 10.1016/j.jastp.2009.03.006

Qian, L., McInerney, J. M., Solomon, S. S., Liu, H., & Burns, A. G. (2021). Climate changes in the upper atmosphere: Contributions by the changing greenhouse gas concentrations and earth's magnetic field from the 1960s to 2010s. *Journal of Geophysical Research: Space Physics*, *126*(3). doi: 10.1029/2020JA029067

Rishbeth, H. (1990). A greenhouse effect in the ionosphere? *Planetary and Space Science*, *38*(7), 945–948. doi: 10.1016/0032-0633(90)90061-T

Rishbeth, H., & Edwards, R. (1989). The isobaric F2-layer. *Journal of Atmospheric and Terrestrial Physics*, *51*(4), 321–338. doi: 10.1016/0021-9169(89)90083-4

Roble, R. G., & Dickinson, R. E. (1989). How will changes in carbon dioxide and methane modify the mean structure of the mesosphere and thermosphere? *Geophysical Research Letters*, *16*(12), 1441–1444. doi: 10.1029/GL016i012p01441

Yue, J., Jian, Y., Wang, W., Meier, R. R., Burns, A., Qian, L., ... Mlynczak, M. (2019). Annual and Semiannual Oscillations of Thermospheric Composition in TIMED/GUVI Limb Measurements. *Journal of Geophysical Research: Space Physics*, *124*(4), 3067–3082. doi: 10.1029/2019JA026544